

Review

LiBH₄ as a Solid-State Electrolyte for Li and Li-Ion Batteries: A Review

Pier Paolo Prosinì

ENEA, Energy Department, C.R. Casaccia, Santa Maria di Galeria, 301, 00123 Roma, Italy;
pierpaolo.prosini@enea.it

Abstract: In this paper, the methods used to enhance the conductivity of LiBH₄, a potential electrolyte for the construction of solid-state batteries, are summarized. Since this electrolyte becomes conductive at temperatures above 380 K due to a phase change, numerous studies have been conducted to lower the temperature at which the hydride becomes conductive. An increase in conductivity at lower temperatures has generally been obtained by adding a second component that can increase the mobility of the lithium ion. In some cases, conductivities at room temperature, such as those exhibited by the liquid electrolytes used in current lithium-ion batteries, have been achieved. With these modified electrolytes, both lithium metal and lithium-ion cells have also been constructed, the performances of which are reported in the paper. In some cases, cells characterized by a high capacity and rate capability have been developed. Although it is still necessary to confirm the stability of the devices, especially in terms of cyclability, LiBH₄-based doped electrolytes could be employed to produce solid-state lithium or lithium-ion batteries susceptible to industrial development.

Keywords: LiBH₄; solid-state electrolyte; batteries; conductivity

1. Introduction

Lithium-ion batteries have made possible a technological leap in the electrification process due to their superior efficiency compared to other types of batteries [1–4]. A further step in the electrification process could be represented by the production of solid-state batteries. In fact, these batteries could have higher safety and stability than current organic liquid electrolyte batteries [5]. The focal point in the development of a solid-state battery is the solid-state electrolyte (SSE). In fact, the SSE must ensure high ionic conductivity and, simultaneously, must be stable with both the anode and the cathode of the battery. Despite the large number of SSEs that have been studied, they can be grouped into three main categories: solid inorganic electrolytes (both ceramic or glass) [6–8], solid polymer electrolytes [9,10], and their hybrids [11,12]. Among them, ceramic/glass materials have proven to be good conductors for lithium ions. These include crystalline [13,14] or glass [15] sulfide, oxides [16], halides [17], and a mixture of metal oxide/metal halides [18,19]. One of the problems that arises due to the use of the ceramic oxide system as an electrolyte in alkaline batteries is correlated to the high resistance of the grain boundary [20]. In fact, these SSEs are manufactured starting from the particles of the respective materials through a hot or cold pressure process. Therefore, their ionic conductivities are usually far lower than those of their bulk phase counterparts [21]. This significant decrease in conductivity is precisely linked to the numerous grain boundaries that are created during the preparation process, which greatly hinder the transfer of lithium ions [22]. This is a common problem for all SSEs, as ion transfer processes typically occur through a short distance hopping mechanism [23]. Furthermore, the SSE can react with the cathode [24] or the anode [25], and this leads to instability in the battery performance. These issues have prompted further efforts to search for a new solid-state electrolytic system.

During their studies on the process of the dehydriding of LiBH₄ by microwave irradiation, Japanese researchers lead by Orimo found that at 380 K, this material undergoes a



Citation: Prosinì, P.P. LiBH₄ as a Solid-State Electrolyte for Li and Li-Ion Batteries: A Review. *Batteries* **2023**, *9*, 269. <https://doi.org/10.3390/batteries9050269>

Academic Editors: Fu Sun and Dengfeng Yu

Received: 2 April 2023

Revised: 27 April 2023

Accepted: 9 May 2023

Published: 12 May 2023



Copyright: © 2023 by the author. Licensee MDPI, Basel, Switzerland. This article is an open access article distributed under the terms and conditions of the Creative Commons Attribution (CC BY) license (<https://creativecommons.org/licenses/by/4.0/>).

reversible phase change from orthorhombic to hexagonal. This phase change is followed by an increase in the conductivity of the material, resulting in a rapid acceleration of the dehydriding rate [26]. Permittivity measurements allowed to understand that LiBH_4 in the orthorhombic phase is an insulator, while it becomes thermally conductive in the hexagonal phase. This allows the hexagonal phase to be heated rapidly, facilitating its dehydriding. Furthermore, since a covalent bond holds hydrogen and boron together to form the borohydride anion whose charge is stabilized by the lithium ion, it has been hypothesized that Li^+ and not H^+ is responsible for the rise in conductivity. This intuition prompted the investigation of LiBH_4 as an ionic conductor for lithium ions.

In the past, LiBH_4 has been used for different applications. LiBH_4 was first synthesized in 1940 by Schlesinger and Brown with the aim of finding new volatile compounds of uranium of low molecular weight for isotopic purification [27]. They first prepared LiBH_4 from diborane B_2H_6 [28] and subsequently extended this procedure in the synthesis of the borohydride of sodium and that of potassium [29]. In addition to their normal use as reducing agents in organic chemistry [30,31], alkali metal borohydrides have found application for hydrogen storage [32,33] because of their extremely high gravimetric hydrogen capacities [34]. The unexpected increase in the thermal conductivity observed in the hexagonal LiBH_4 opened a new field of applications for this material as an ionic conductor for lithium ions. Indeed, the ionic conductivity measures have shown that, for temperatures above 380 K, this compound has an electric conductivity like that of liquid electrolytes [35]. The discovery of the high electric conductivity of LiBH_4 has opened the field to numerous studies on the conduction properties of various borohydrides and the mixture of these with other compounds to increase their ionic conductivity [36]. In this review, the main results obtained in relation to using borohydride-based materials as SSEs for alkali metal batteries are reported.

2. Solid-State Electrolytes

In the original work of Orimo [35], the conductivity of LiBH_4 was measured before and after the phase change. For both phases, the frequency response in the impedance graphs shows the presence of a single arc. This means that the response deriving from the electrode/electrolyte interface and that relating to the grain boundary are both absent. The resistance measured at 337 K, i.e., before the phase transition temperature, was over 6000 ohms. After increasing the temperature to 391 K, the resistance dropped to only 170 ohms. The electrical conductivity calculated for the hexagonal phase was $10^{-3} \text{ S cm}^{-1}$, which is like that of the liquid electrolytes used in current lithium-ion batteries measured at ambient temperature. For both phases, the temperature dependencies of the electrical conductivity showed a typical Arrhenius behavior. The calculated activation energies were 0.69 and 0.53 eV for the orthorhombic and hexagonal phases, respectively. ^7Li NMRs produced conductivity data that showed a good agreement with the electrical conductivity measured by impedance spectroscopy, confirming that the high electrical conductivity originates from the fast Li ion motion. The ^1H and ^{11}B nuclear magnetic resonance spectra were used to investigate the rotational movement of BH_4 tetrahedra in LiBH_4 [37]. It was observed that the low temperature phase (orthorhombic) presents the coexistence of two kinds of rotary movement of BH_4 tetrahedra, with two distinct activation energies. The jump rates of reorientation, for both types of motion, have values of about 10^{11} s^{-1} . The LiBH_4 phase change from orthorhombic to hexagonal, which occurs at a high temperature, leads to a large increase in the spin lattice relaxation time. A further low frequency fluctuation process is observed in the high temperature phase, and both the relaxation rates of the ^1H and ^{11}B spin lattice are governed by a characteristic rate of four orders of magnitude lower (10^7 s^{-1}) than the orthorhombic phase, probably due to the translational spread of the Li ions.

Numerous studies have been conducted to try to decrease the temperature at which the phase transition occurs. To stabilize the room-temperature hexagonal phase of LiBH_4 , lithium halides [38], lithium sulfide/phosphorous sulfide [39], and lithium chloride/phosphorous

sulfide [40] were added to the hydride. Carbon and silicon-based materials such as fullerene [41,42], silicon oxide [43–45], and mesoporous silica [46,47], which were eventually added with lithium iodide [48,49], were also employed. Low molecular weight molecules including water [50] and ammonia [51–53], which were eventually added with silicon oxide [54], lithium amide [55,56], ammonia borane [57], mono-methylamine [58], oxygen [59], magnesium oxide [60], lithium tetrafluoro borate [61], and lithium thiophosphate [62] were also used to increase the conductivity of the hydride at lower temperatures.

It has been found that the addition of lithium halides resulted in a substantial decrease in the transition temperature [38]. Among all halides, the LiI-doped one showed the most significant decrease in the transition temperature. For this sample, a conductivity of $1.0 \times 10^{-3} \text{ S cm}^{-1}$ was calculated at $50 \text{ }^\circ\text{C}$ (Figure 1). Both NMR and XRD showed room-temperature stabilization of the superionic phase for LiI-doped LiBH_4 .

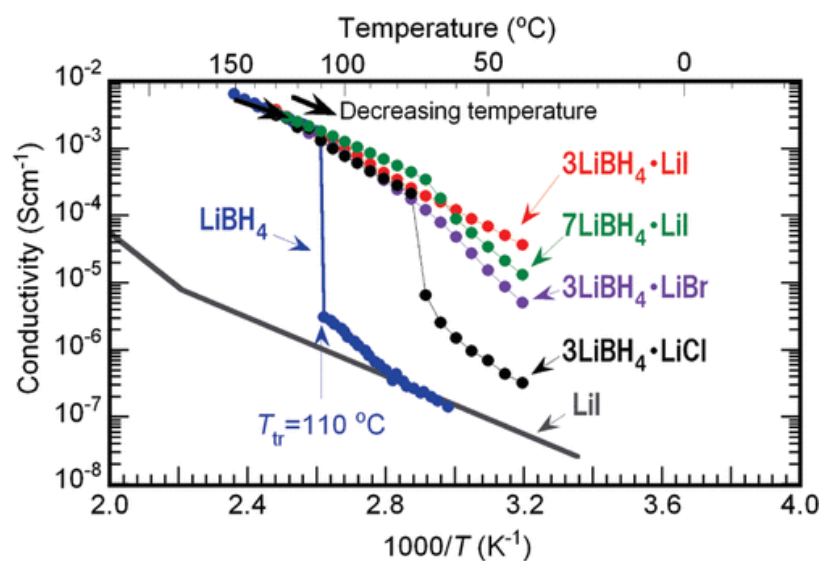


Figure 1. Specific conductivities of pure or doped with lithium halides LiBH_4 obtained by AC impedance as a function of temperature. Reproduced with permission from ref. [38]. Copyright 2009 American Chemical Society.

To improve the conduction properties of $\text{P}_2\text{S}_5\text{-Li}_2\text{S}$ glasses, it has been hypothesized to add LiBH_4 to the sulfide-based electrolytes [39]. The conductivity of the glasses was observed to increase with raising the LiBH_4 amount. A conductivity as high as $1.6 \times 10^{-3} \text{ S cm}^{-1}$ was exhibited by the sample containing 33 mol% LiBH_4 . The study on $\text{LiBH}_4\text{-P}_2\text{S}_5\text{-LiCl}$ composites showed that this material undergoes amorphization at $60 \text{ }^\circ\text{C}$, accompanied by an increase in Li^+ conduction [40]. The ionic conductivity of the optimized borohydride-sulfide-halide system is approximately $10^{-3} \text{ S cm}^{-1}$ at ambient temperature. Furthermore, the activation energy for ion migration is low. This makes it suitable for building solid-state batteries that operate near room temperature.

Moreover, the addition of fullerene significantly enhances the conductivity of LiBH_4 . The mobility of the lithium ions was further increased after thermal annealing reached a value comparable to that observed for the lithium halides. A lithium ionic conductivity of $2.0 \times 10^{-5} \text{ S cm}^{-1}$ at $25 \text{ }^\circ\text{C}$ that increased up to $2.0 \times 10^{-3} \text{ S cm}^{-1}$ at $140 \text{ }^\circ\text{C}$ was observed in an annealed sample containing 30 wt.% of fullerenes [41] (Figure 2). The improvement of the ionic conductivity of fullerene-added LiBH_4 was also achieved through a partial dehydrogenation achieved by heating [42].

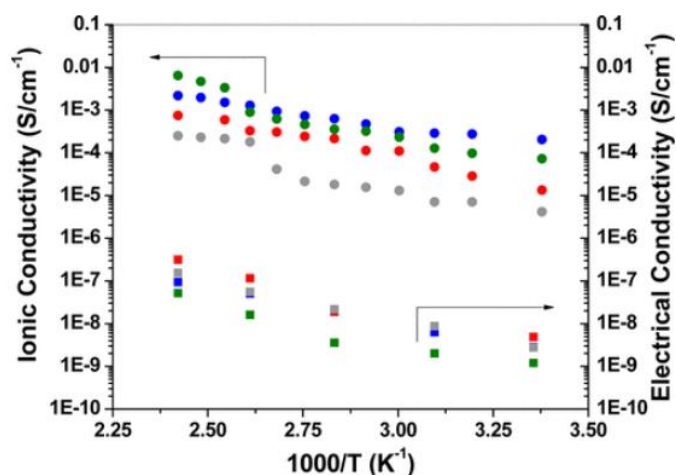


Figure 2. Electrical (■) and ionic (●) conductivity measurements of the $\text{LiBH}_4\text{:C}_{60}$ nanocomposites. Red— $\text{LiBH}_4\text{:C}_{60}$ (70:30) as prepared; blue— $\text{LiBH}_4\text{:C}_{60}$ (70:30) annealed at 300 °C; gray— $\text{LiBH}_4\text{:C}_{60}$ (50:50) as prepared; green— $\text{LiBH}_4\text{:C}_{60}$ (50:50) annealed at 300 °C. Reproduced with permission from ref. [41]. Copyright 2021 American Chemical Society.

Even more impressive was the effect on the structural phase transition, Li ion mobility, and ionic conductivity of the nanoconfinement of LiBH_4 in ordered mesoporous SiO_2 scaffolds. At 40 °C, the conductivity of the composite was $1.20 \times 10^{-4} \text{ cm}^{-1}$, with a three-order-of-magnitude increase when compared to the pristine LiBH_4 at the same temperature [43] (Figure 3).

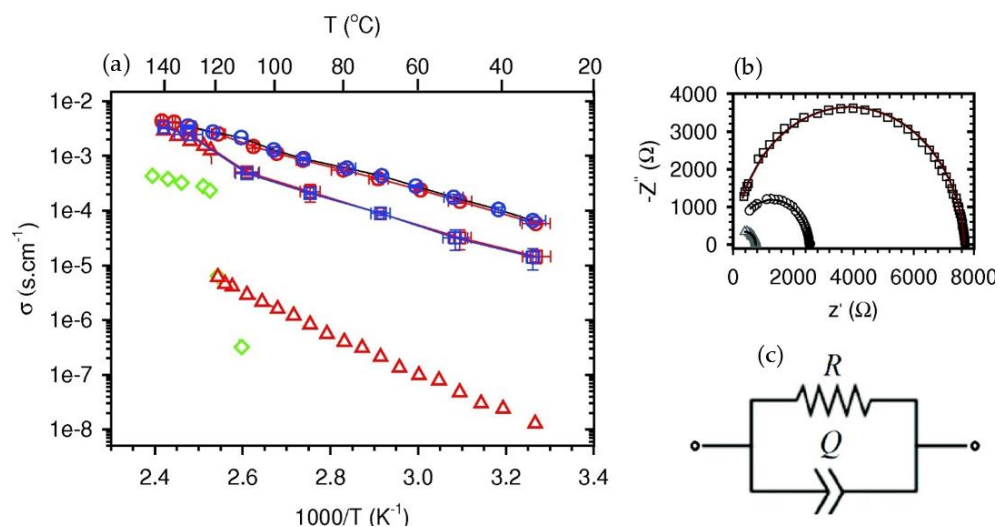


Figure 3. (a) Temperature dependence of ionic conductivity of $\text{SiO}_2\text{-LiBH}_4$ nanocomposites and pristine LiBH_4 . All nanocomposites contained 42 wt.% LiBH_4 , but the degrees of pores filling are different. Red triangles: pristine LiBH_4 , circles, and squares: sample melt-infiltrated, green diamonds: physical-mixture, (b) Nyquist plot obtained for the impedance measurements at various temperatures (squares: 30 °C, circles: 50 °C, triangles: 80 °C). (c) equivalent circuit used to fit the electrochemical impedance spectroscopy data. Reproduced with permission from ref. [43]. Copyright 2015 Wiley.

The ^7Li and ^{11}B spectra of LiBH_4 contained in orderly porous silica (pore size MCM-41: 1.9 nm) showed, in addition to the bulk-like resonance of LiBH_4 , a narrower additional part [44]. Above $T = 313 \text{ K}$, this part showed a typical J-coupling pattern in both ^{11}B and ^1H spectra. The observed J-coupling pattern can be traced back to the presence of highly mobile BH_4^- species. Static measurements have confirmed that the BH_4^- mobility in LiBH_4 is greatly improved by nanoconfinement. At the same time, there is a significant

enhancement in the mobility of Li^+ . These J-coupling patterns due to highly mobile species can also be observed in the molten LiBH_4 . This means that nanoconfinement strongly enhances the mobility of borohydride anions in LiBH_4 . By decreasing the temperature, the J-coupling pattern vanishes due to the reduction in mobility. Since the narrowing of the line already occurs far below the phase transition temperature and far below the melting point of LiBH_4 , it follows that nanoconfinement can stabilize the high-temperature phase already at room temperature.

The confinement of LiBH_4 in silica characterized by different degrees of porosity has been studied in [45] using micro- SiO_2 , porous nano- SiO_2 , and nano- SiO_2 with nanochannels as supports (Santa Barbara Amorphous-15, SBA-15). All LiBH_4 /silica composites exhibited ionic conductivity superior to that of the silica-free material. LiBH_4 /SBA-15 (at a weight ratio of 47%) exhibited the highest conductivity of $3.0 \times 10^{-5} \text{ S cm}^{-1}$ at 35°C , with a three-order-of-magnitude increase compared to that of pure LiBH_4 . The LiBH_4 /SBA-15 composite also exhibited an electrochemical stability window extending from -0.2 to 5.0 V . A. Further investigation on SBA-15 studied the effect of the preventive heat treatment of SBA-15 on the performance of the solid electrolyte obtained by infiltrating the silica nanochannels with LiBH_4 [46]. SBA-15 was previously dried for 6 h at a certain temperature (from ambient temperature up to 600°C). The preparation of the nanocomposites was achieved by melt infiltration. Figure 4 illustrates the behavior of the conductivity as a function of temperature for the LiBH_4 infiltrated inside the silica mesopores: values ranged between 10^{-6} and $10^{-5} \text{ S cm}^{-1}$ at 30°C . The difference in the conductivity values was related to the different thermal treatments undergone by the silica before melt infiltration. The Nyquist plot for the SiO_2 sample heated at 300°C displays a single semi-circle, which is typical of conductivity phenomena characterized by a single process. For this sample, the specific conductivity measured at 30°C was $5.0 \times 10^{-6} \text{ S cm}^{-1}$.

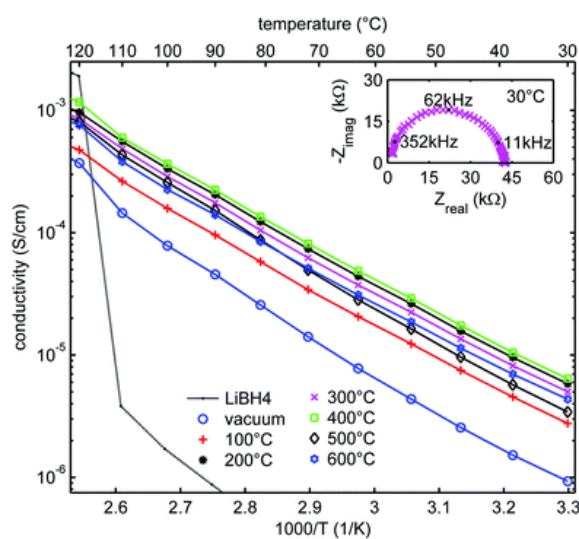


Figure 4. Graphs showing ionic conductivity as a function of temperature for LiBH_4 /SiO₂ nanocomposites (for more details see ref. [46]). The insert shows the Nyquist graph of the impedance measurement carried out at 30°C . Reproduced from ref. [46] under Creative Commons Attribution License. Copyright 2015 Royal Society of Chemistry.

SBA-15 with various pore sizes infiltrated with LiBH_4 was studied using ^1H , $^6,7\text{Li}$, and ^{11}B solid-state NMR at different temperatures [47]. To interpret the obtained results, it was hypothesized that the LiBH_4 inside the pores is in a bulk form detached from the pore walls by a highly dynamic amorphous fraction. The percentage of dynamic fraction rises by increasing the temperature. The exchange of lithium ions between the two fractions is slow at room temperatures, but beyond the temperature at which the phase transition of the innermost fraction takes place, the lithium ions can diffuse rapidly through both fractions.

Therefore, no increase in ion mobility is noted at room temperature. When the temperature is increased, the material confined within the pores undergoes the phase transition and all Li ions are highly mobile. Consequently, all Li ions confined in the nanopores look like a single highly dynamic element in the NMR spectra.

When the LiBH_4 was doped with LiI before being introduced into the nanopores of the SBA-15, a highly conductive Li-ion electrolyte was obtained [48]. $\text{Li}_4(\text{BH}_4)_3\text{I}@SBA-15$ was prepared by the partial exchange of I^- for BH_4^- to form $\text{Li}_4(\text{BH}_4)_3\text{I}$, which was obtained by heating LiBH_4 and LiI at 250°C and 100 bars of hydrogen for 12 h. Then, the SBA-15 was filled with $\text{Li}_4(\text{BH}_4)_3\text{I}$ by heating the mixtures $\text{Li}_4(\text{BH}_4)_3\text{I}$ and SBA-15 for 1 h at 340°C under 130 bars of hydrogen, as schematically shown in Figure 5. The uniform nanoconfinement of the LiBH_4/LiI mixture in the silica mesopores leads to an electrolyte with a conductivity of $2.5 \times 10^{-4} \text{ S cm}^{-1}$ at 35°C . At the same temperature, the Li ion transfer number was calculated to be 0.97. This high conductivity is probably attributable to the higher mobility of the lithium ions in the interface layer between the $\text{Li}_4(\text{BH}_4)_3\text{I}$ and the mesoporous silica. In addition, this electrolyte has a higher dendrite suppression capability, with a critical current density of 2.6 mA cm^{-2} at 55°C and an electrochemical stability window that extended up to 5.0 V.

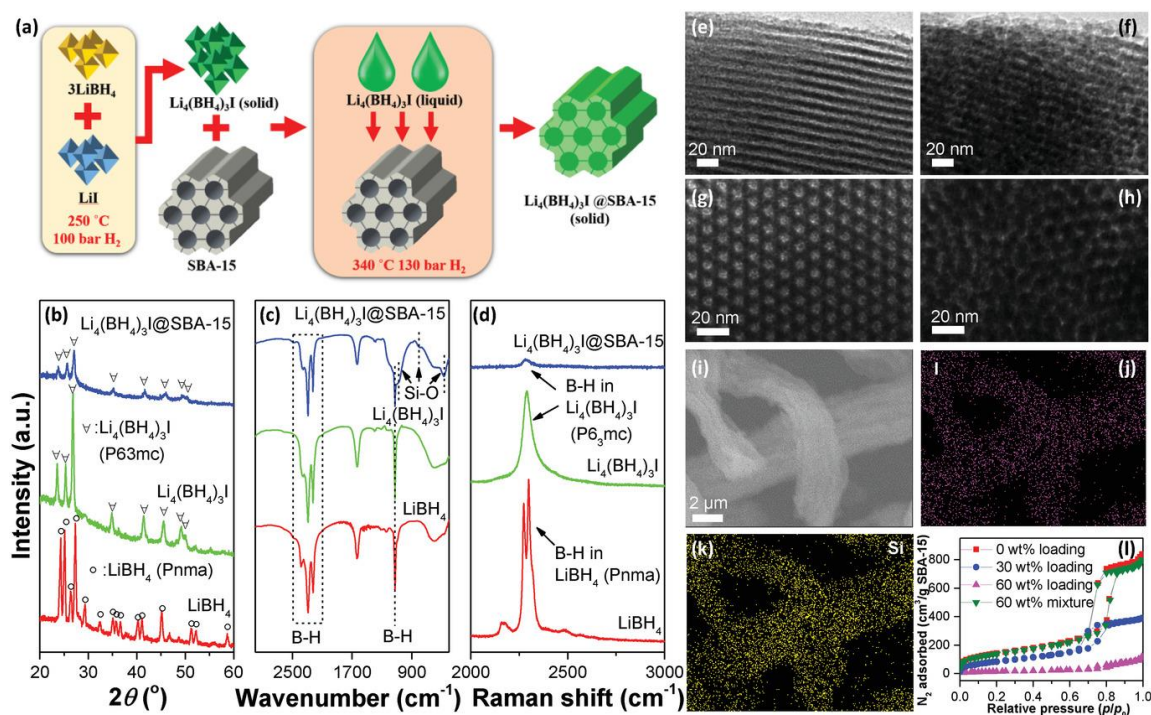


Figure 5. (a) An explanatory scheme of the preparation process of $\text{Li}_4(\text{BH}_4)_3\text{I}$ in SBA-15; (b) X-ray diffractograms, (c) FTIR spectra, (d) Raman spectra of LiBH_4 , $\text{Li}_4(\text{BH}_4)_3\text{I}$, and $\text{Li}_4(\text{BH}_4)_3\text{I}@SBA-15$; TEM images of (e,g) SBA-15 and (f,h) $\text{Li}_4(\text{BH}_4)_3\text{I}@SBA-15$; (i–k) SEM-EDS images of $\text{Li}_4(\text{BH}_4)_3\text{I}@SBA-15$; (l) nitrogen adsorption isotherms of SBA-15, $\text{Li}_4(\text{BH}_4)_3\text{I}@SBA-15$, and $\text{Li}_4(\text{BH}_4)_3\text{I}/SBA-15$. Reproduced with permission from ref. [48]. Copyright 2019 Wiley.

Solid polymer electrolytes were obtained through a casting method in liquid solution. $\text{LiBH}_4/\text{Li}_4(\text{BH}_4)_3\text{I}$ and poly(ethylene oxide) (PEO), with or without SiO_2 , were dissolved in anhydrous acetonitrile, and after 20 h of stirring, the solution was poured onto a PTFE film. After the evaporation of acetonitrile at room temperature, the solid polymer electrolyte membrane was formed. The composite solid polymer electrolyte $\text{PEO}_{10}\text{-Li}_4(\text{BH}_4)_3\text{I}$ containing 5 wt.% SiO_2 exhibited a lithium-ion conductivity of $4.28 \times 10^{-4} \text{ S cm}^{-1}$ at 70°C that resulted higher than plain LiBH_4 or the pure electrolyte PEO-LiBH_4 [49].

Water content has also been found to influence the transport properties of LiBH_4 . LiBH_4 can incorporate water without decomposing. The process is reversible and structural

water can be lost at 55 °C. In its hydrated form, the lithium-ion conductivity of LiBH_4 at 45 °C is $4.89 \times 10^{-4} \text{ S cm}^{-1}$ [50]. The ^7Li NMR spectra obtained when the LiBH_4 hydrate is heated around the dehydration temperature indicate that the increase in the conductivity of the lithium ions could be related to the movement of structural water.

Several works have dealt with the doping of LiBH_4 with ammonia or its derivatives. The various LiBH_4 ammoniates can easily be synthesized by varying the amount of ammonia supplied to the LiBH_4 at ambient temperature. Salts of general formula $\text{Li}(\text{NH}_3)_n\text{BH}_4$ ($0 < n \leq 2$) have shown conductivities of the order of $10^{-3} \text{ S cm}^{-1}$ for temperatures below 40 °C [51]. The electric properties of the lithium borohydride ammoniates are illustrated in Figure 6. These compounds have been proposed as SSE, although further studies are necessary to use this ammonia complex for practical application. More recently, the lithium borohydride hemiamine, $\text{LiBH}_4 \cdot 1/2\text{NH}_3$, was investigated, for which a new Li^+ conductivity pathway was supposed [52]. The addition of ammonia for every two moles of LiBH_4 causes an increase in conductivity, reaching $7.0 \times 10^{-4} \text{ S cm}^{-1}$ at 40 °C in the solid state and increasing to $3.0 \times 10^{-2} \text{ S cm}^{-1}$ at 55 °C after melting.

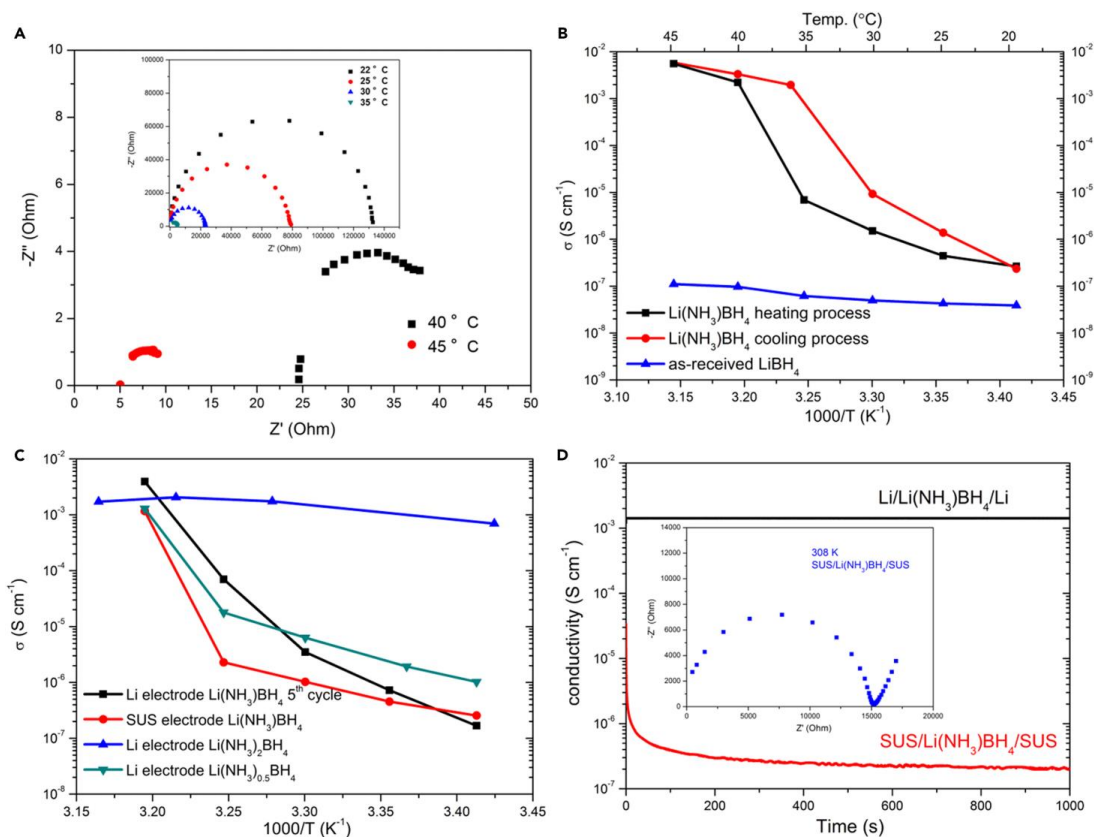


Figure 6. (A) Nyquist plots obtained by heating the electrolyte from 20 °C to 45 °C between two lithium electrodes. (B) The ionic conductivity of the ammonia complex under heating (black) and cooling (red) of the pristine LiBH_4 (blue). (C) Lithium ion conductivity of samples: $\text{Li}(\text{NH}_3)\text{BH}_4$ for the fifth cycle (black), steel electrode $\text{Li}(\text{NH}_3)\text{BH}_4$ (red), $\text{Li}(\text{NH}_3)\text{BH}_4$ (blue), and $\text{Li}(\text{NH}_3)_{0.5}\text{BH}_4$ (dark cyan). (D) DC conductivity of $\text{Li}(\text{NH}_3)\text{BH}_4$ obtained after applying a constant voltage of 0.1 V to the steel and lithium electrodes at 40 °C, respectively. The box shows the impedance graph obtained using a steel electrode at 35 °C. Reproduced with permission from ref. [51]. Copyright 2019 Elsevier.

Composites, prepared by a ball milling process and having the general formula $\text{LiBH}_4 \times \text{NH}_3 \cdot \text{Li}_2\text{O}$, were obtained using LiBH_4 , LiNH_2 , and LiOH as precursors [53]. During the process, $\text{LiBH}_4 \times \text{NH}_3$ transforms into an amorphous material and the ionic conductivity at 20 °C rises to $5.4 \times 10^{-4} \text{ S cm}^{-1}$. Composites of LiBH_4 containing ammonia and silicon oxide were also prepared [54]. Composites of formula $\text{Li}(\text{NH}_3)_x\text{BH}_4 @ \text{SiO}_2$ ($0 \leq x \leq 0.5$)

were prepared by absorbing ammonia into LiBH_4 and incorporating silicon oxide by ball milling. Among the different prepared materials, the $\text{Li}(\text{NH}_3)_{0.5}\text{BH}_4@/\text{SiO}_2$ showed an ionic conductivity of $3.95 \times 10^{-2} \text{ S cm}^{-1}$ at 60°C . The ionic conductivity at 40°C in lithium amide-borohydride was found to be $6.4 \times 10^{-3} \text{ S cm}^{-1}$ [55]. The materials of formula $\text{Li}(\text{BH}_4)_{1-x}(\text{NH}_2)_x$ were prepared using LiBH_4 and LiNH_2 as precursors [56]. Reactive ball milling followed by a heat treatment at 120°C was used to prepare the materials. A conductivity of $2.0 \times 10^{-4} \text{ S cm}^{-1}$ at 40°C was calculated for the reference sample ($x = 3/4$), with an activation energy of 0.34 eV. By increasing the LiBH_4 : LiNH_2 precursor ratio to 1:2 ($x = 2/3$), an increase in conductivity was found. The conductivity increased by more than one order of magnitude, reaching $6.4 \times 10^{-3} \text{ S cm}^{-1}$ at 40°C . The incorporation of ammonia borane (AB) into the LiBH_4 facilitates the conduction of lithium ions due to the increase in cell volume and, consequently, the decrease in volumetric density [57]. At 25°C , the $\text{LiBH}_4 \cdot \text{AB}$ complex showed ionic conductivities of the order of $4.04 \times 10^{-4} \text{ S cm}^{-1}$. The Li-ion transfer number measured at 40°C was greater than 0.999. To explain these performances, ab initio molecular dynamics simulations have been carried out which show the presence, along the b direction in the $\text{LiBH}_4 \cdot \text{AB}$ structure, of a 1D diffusion channel, which presents a very low activation energy barrier (0.12 eV), consequently allowing for the higher conductivity of Li ions at 25°C . The addition of mono-methylamine to LiBH_4 leads to the formation of the crystalline complex $\text{LiBH}_4 \cdot \text{CH}_3\text{NH}_2$ which crystallizes in the monoclinic space group $\text{P}21/c$, to which corresponds a two-dimensional layered structure that allows for the rapid movement of Li ions at room temperature [58]. The layers are separated by $-\text{CH}_3$ groups, resulting in the formation of large voids (Figure 7). These spaces allow for the rapid passage of Li ions, enabling the material to reach a conductivity of $1.24 \times 10^{-3} \text{ S cm}^{-1}$ at room temperature. Unfortunately, the electrochemical stability is limited to about 2.1 V vs. Li.

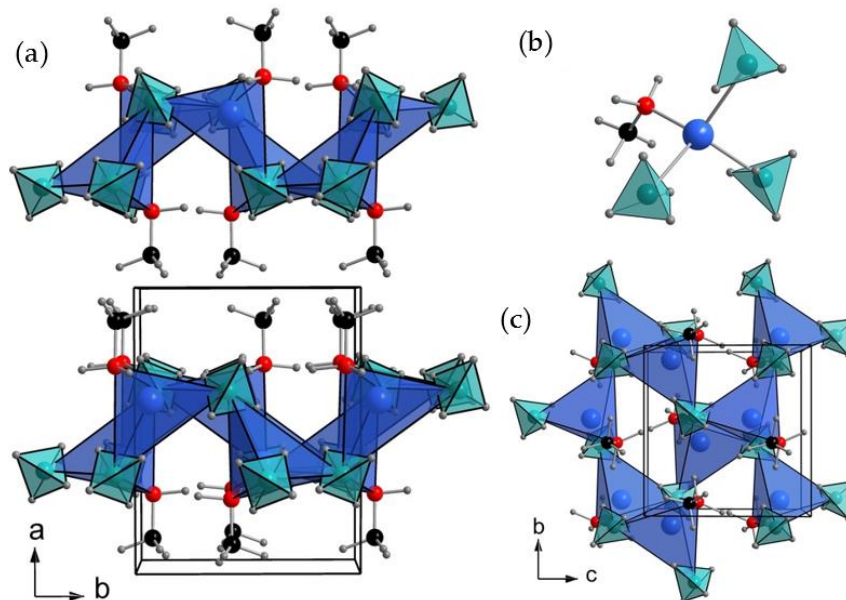


Figure 7. Crystalline structure of $\text{LiBH}_4 \cdot \text{CH}_3\text{NH}_2$. (a) The layers observed from the ab -plane, (b) the Li coordination, and (c) the layer observed in the bc -plane. Color combination: H (gray), Li^+ (blue), C (black), N (red), and BH_4^- (light blue tetrahedra). Reproduced with permission from ref. [58]. Copyright 2022 Wiley.

A quick and easy method of activating LiBH_4 to significantly increase its conductivity is to expose the borohydride to oxygen [59]. This exposure determines the oxidation of the borohydride particles placed on the surface. The rearrangement of the surface atoms results in defects that strongly increase the ionic conductivity. Oxidized LiBH_4 shows a conductivity value at 35°C equal to $1.97 \times 10^{-4} \text{ S cm}^{-1}$, which is five orders of magnitude

higher than that of the pristine LiBH_4 . At 55°C , the ionic conductivity of the oxidized LiBH_4 reached $1.88 \times 10^{-3} \text{ S cm}^{-1}$, one of the highest ionic conductivities reported so far for solid-state electrolytes based on this material. A similar increase in conductivity was also found for the $\text{Mg}(\text{BH}_4)_2$ (Figure 8).

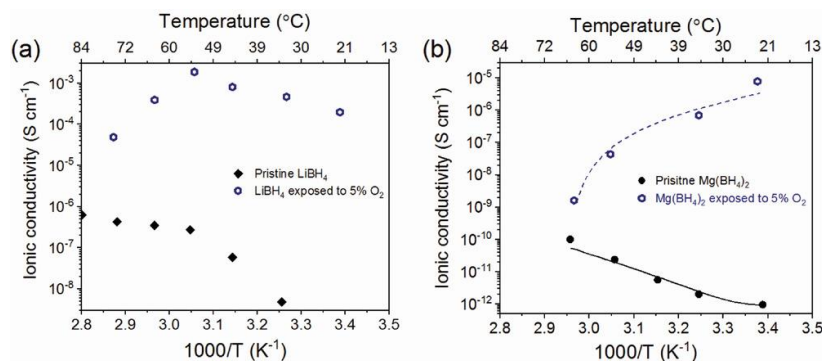


Figure 8. Arrhenius plot of (a) LiBH_4 exposed to 5% O_2 versus that of uncontaminated LiBH_4 , and (b) $\text{Mg}(\text{BH}_4)_2$ exposed to 5% O_2 versus that of uncontaminated $\text{Mg}(\text{BH}_4)_2$. Reproduced with permission from ref. [59]. Copyright 2020 Wiley.

To improve the conductivity of Li ions, MgO was added to LiBH_4 [60] and different compositions were tested. Among these, the mixture containing 53 $v/v\%$ of MgO exhibited the highest conductivity equal to $2.86 \times 10^{-4} \text{ S cm}^{-1}$ at 20°C . The use of MgO had no effect on the extension of the electrochemical stability window, which was about 2.2 V vs. Li^+/Li .

LiBH_4 reacts with LiBF_4 , with the in-situ formation of LiF and lithium closoborates [61]. The formation of these compounds leads to the creation of highly conductive interfaces within the decomposed LiBH_4 structure. As a result, there is an increase in the ionic conductivity, which reaches a value of $0.9 \times 10^{-5} \text{ S cm}^{-1}$ at 30°C .

A solid electrolyte characterized by a high conductivity at ambient temperature was obtained by mixing lithium thiophosphate with LiBH_4 [62]. The preparation method is extremely simple as it consists of grinding the two compounds without any heat treatment. The solid electrolyte shows an ionic conductivity of $11 \times 10^{-3} \text{ S cm}^{-1}$ at 25°C (Figure 9). Despite the studies performed, the mechanism of action of thiosulfate in increasing the ionic conductivity of LiBH_4 still remains unclear.

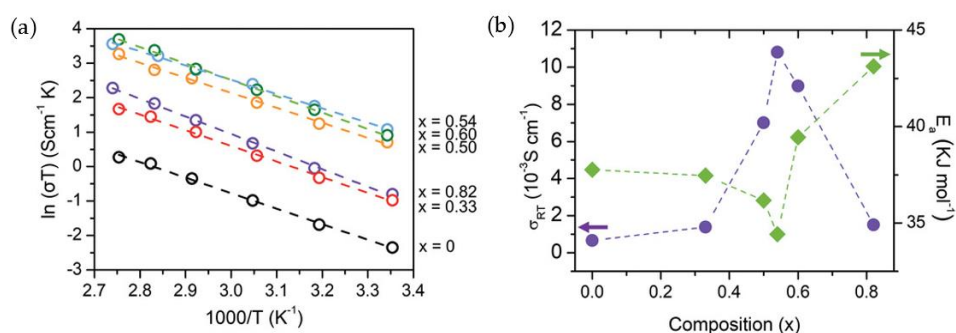


Figure 9. (a) Variation of the ionic conductivities with temperature and (b) activation energy and ionic conductivity at 25°C of the solid electrolyte samples, with various compositions of $(1-x)\text{Li}_3\text{PS}_4 \cdot 2x\text{LiBH}_4$. Reproduced under Creative Commons Attribution License from ref. [62]. Copyright 2023 Wiley.

3. Lithium Metal Batteries

Several different materials, such as TiS_2 [39], LiCoO_2 [63], $\text{LiNi}_{1/3}\text{Mn}_{1/3}\text{Co}_{1/3}\text{O}_2$ [64], $\text{Li}_4\text{Ti}_5\text{O}_{12}$ [55], S [65,66], LiFePO_4 [42], and $\text{LiNi}_{0.7}\text{Mn}_{0.15}\text{Co}_{0.15}\text{O}_2$ [62], have been studied

as the cathode for LiBH_4 -based SSE batteries. The 33 mol % LiBH_4 - Li_2S - P_2S_5 glass was coupled with TiS_2 to assemble an all-solid-state lithium cell [39]. The voltage profiles of the first five cycles conducted at a current density of 0.064 mA cm^{-2} at room temperature are shown in Figure 10. The first cycle discharge capacity was about 223 mAh g^{-1} , which corresponds to 93% of the theoretical capacity of TiS_2 . In subsequent cycles, a slight loss of capacity was observed. Despite that, the cell exhibited a capacity of about 200 mAh g^{-1} , with a Coulombic efficiency of over 99% in the following cycles.

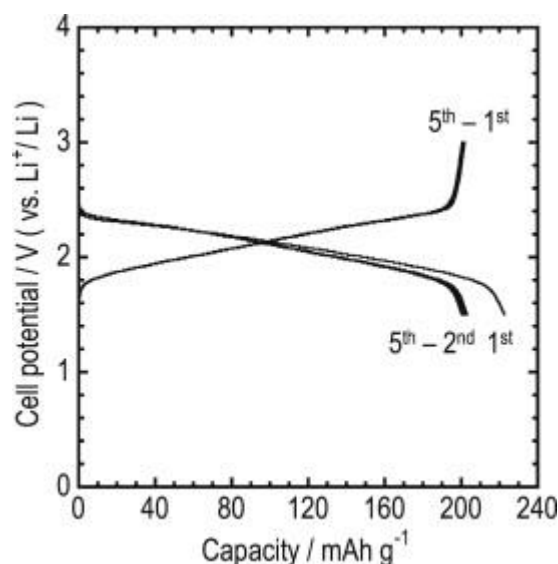


Figure 10. Voltage profiles of a solid-state Li/TiS_2 cell with glass electrolyte $67(0.75\text{Li}_2\text{S } 0.25\text{P}_2\text{S}_5)$ 33LiBH_4 cycled at a current density of 0.064 mA cm^{-2} at 25°C . Reproduced with permission from ref. [39]. Copyright 2013 Elsevier.

The LiCoO_2 was cycled at a temperature above the LiBH_4 transition temperature (120°C) [63]. During the first cycle, the cell showed a charge capacity of 157 mAh g^{-1} , which approximates the theoretical capacity of LiCoO_2 . Unfortunately, in the following cycles, a strong capacity fading reduced the capacity, which was as low as 18 mAh g^{-1} at the tenth cycle. Impedance spectroscopy showed a progressive increase in the charge transfer resistance. As the chemical compatibility of LiBH_4 with a lithium electrode has been proven to be good, the increase in resistance was attributable to cathode degradation. The formation of an insulating layer at the interface between the cathode material and LiBH_4 has been implicated as the cause of the degradation that occurs as the cycle progresses. To reduce the capacity loss, a thin layer of Li_3PO_4 , LiNbO_3 , and Al_2O_3 was used to coat the cathode material [67]. The interfacial resistance was effectively reduced by applying a 10–25 nm thick Li_3PO_4 interlayer. The cell, discharged at a current density of 0.05 mA cm^{-2} , exhibited a discharge capacity of 89 mAh g^{-1} and maintained about 97% of the initial capacity after 30 full charge–discharge cycles. The cell made with $\text{LiNi}_{1/3}\text{Mn}_{1/3}\text{Co}_{1/3}\text{O}_2$ also exhibited an increase in the contact resistance as cycling progressed [57]. The contact resistance was reduced by using an adhesive layer formed by a mixture of LiBH_4 and LiNH_2 . Thanks to the presence of this barrier layer, repeated charge–discharge cycles have been obtained. At the first cycle, the cell heated to 150°C showed a discharge capacity of 114 mAh g^{-1} . After ten cycles, the capacity was about 71% of the initial one.

The lithium amide-borohydride electrolyte was tested using a $\text{Li}_4\text{Ti}_5\text{O}_{12}$ electrode. The cell exhibited high bulk and interfacial stability, good rate capability, and an extended cycle life [55]. The cell cycled for 400 cycles at 0.7 mA cm^{-2} (1 C) and retained good capacity up to 3.5 mA cm^{-2} (5 C) at 40°C (Figure 11).

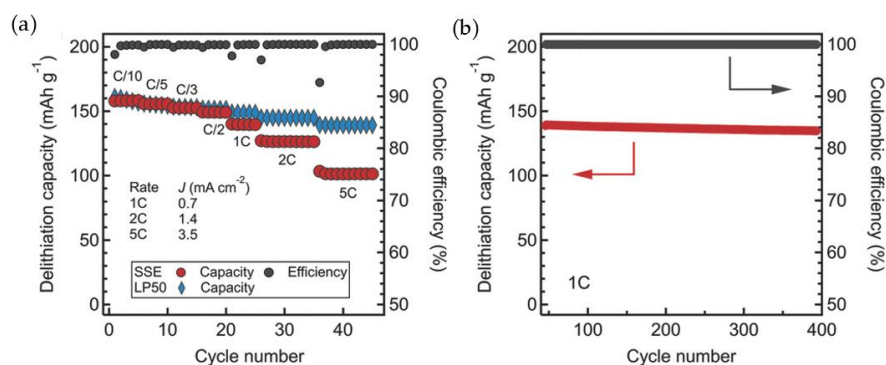


Figure 11. $\text{Li}_4\text{Ti}_5\text{O}_{12}$ /lithium cell using $\text{Li}(\text{BH}_4)_{1-x}(\text{NH}_2)_x$ ($x = 2/3$) as SSE tested at 40°C . (a) Discharge capacities and Coulombic efficiencies at different rates for a cell with the SSE. For comparison, a cell using LP50 as the liquid electrolyte is shown. (b) Capacity as a function of the number of cycles for the SSE cell cycled at 1C. Reproduced with permission from ref. [55]. Copyright 2017 Wiley.

A composite cathode of sulfur-infiltrated carbon nanotubes was employed to make a solid-state Li/S battery [65]. LiBH_4 was used as SSE. The cathode exhibited an initial capacity of 1459 mAh g^{-1} . As cycling progressed, the specific capacity faded to a constant value of 398 mAh g^{-1} .

A composite material obtained by mixing sulfur and graphene oxide (GO) or reduced graphene oxide (rGO) in a percentage of 1 or 10% [66] was tested as the positive active material of a solid-state battery. The cells were tested at 20°C and a 0.1C rate. The cell containing 1%GO-99%S exhibited a first cycle capacity of 1100 mAh g^{-1} , while in the subsequent charge, it managed to accumulate 1700 mAh g^{-1} (Figure 12). Probably during the heating process, the sulfur and the LiBH_4 (present as SSE in the cathode formulation) reacted to form Li_2S . Therefore, not all the sulfur that was initially present in the cathode was available for the electrochemical reaction. This explains why the initial capacity was lower than the theoretical capacity. While charging, the cell provided a capacity higher than the theoretical one (1675 mAh g^{-1}), probably following the reaction between the sulfur and the LiBH_4 . A severe capacity fading was observed in subsequent cycles and the capacity decreased to a constant value of approximately 150 mAh g^{-1} after 42 cycles. The same behavior was observed for the 10%GO-90%S composite. The cell showed a first cycle specific capacity of 1309 mAh g^{-1} and 1165 mAh g^{-1} in charge and discharge, respectively, with a Coulomb efficiency of about 89%. The capacity retention with cycling was poor since the capacity strongly reduced after a few cycles.

Using a composite of formula $\text{Li}(\text{NH}_3)0.5\text{BH}_4@\text{SiO}_2$ as an electrolyte, a lithium-sulfur solid-state cell was constructed, which exhibited a specific discharge capacity of 1221.7 mAh g^{-1} after 10 cycles [54]. The cell also showed good rate capability. The cell managed to discharge 1589 mAh g^{-1} at 0.1C and 695 mAh g^{-1} when discharged at C rate. Before realizing the complete cell, the stability of $\text{Li}(\text{NH}_3)0.5\text{BH}_4@\text{SiO}_2$ against metallic lithium was studied. As shown in Figure 13a–d, it emerged that the $\text{Li}/\text{Li}(\text{NH}_3)0.2\text{BH}_4/\text{Li}$ cell had low ionic conductivity at low temperatures (30°C and 40°C). At higher temperatures (50°C), the melting of the electrolyte (Figure 13a–d, digital images) was observed. However, the charge-discharge curves of the $\text{Li}/\text{Li}(\text{NH}_3)0.5\text{BH}_4@\text{SiO}_2/\text{Li}$ symmetrical cell at 0.1 mA cm^{-2} show regular cycles, with no short-circuit formation after 100 h. $\text{Li}/\text{Li}(\text{NH}_3)0.5\text{BH}_4@\text{SiO}_2/\text{S}$ cells were then fabricated and cycled at 0.2C, which showed second cycle specific capacities of 818.7 mAh g^{-1} and 777 mAh g^{-1} at 40°C and 50°C , respectively (Figure 13e). The cell has been shown to work very well at various temperatures (Figure 13f) and discharge rates (Figure 13g).

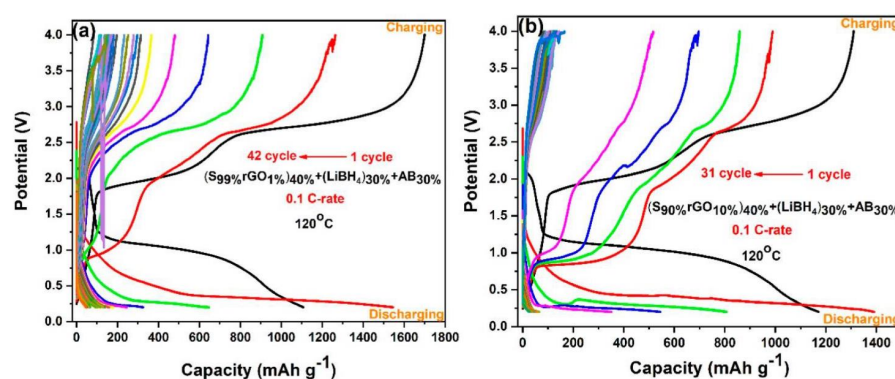


Figure 12. (a) Voltage profiles of the S99%rGO1% electrode. (b) Voltage profiles of the S90%rGO10% electrode. Reproduced from ref. [66] under Creative Commons Attribution License. Copyright 2021 MDPI.

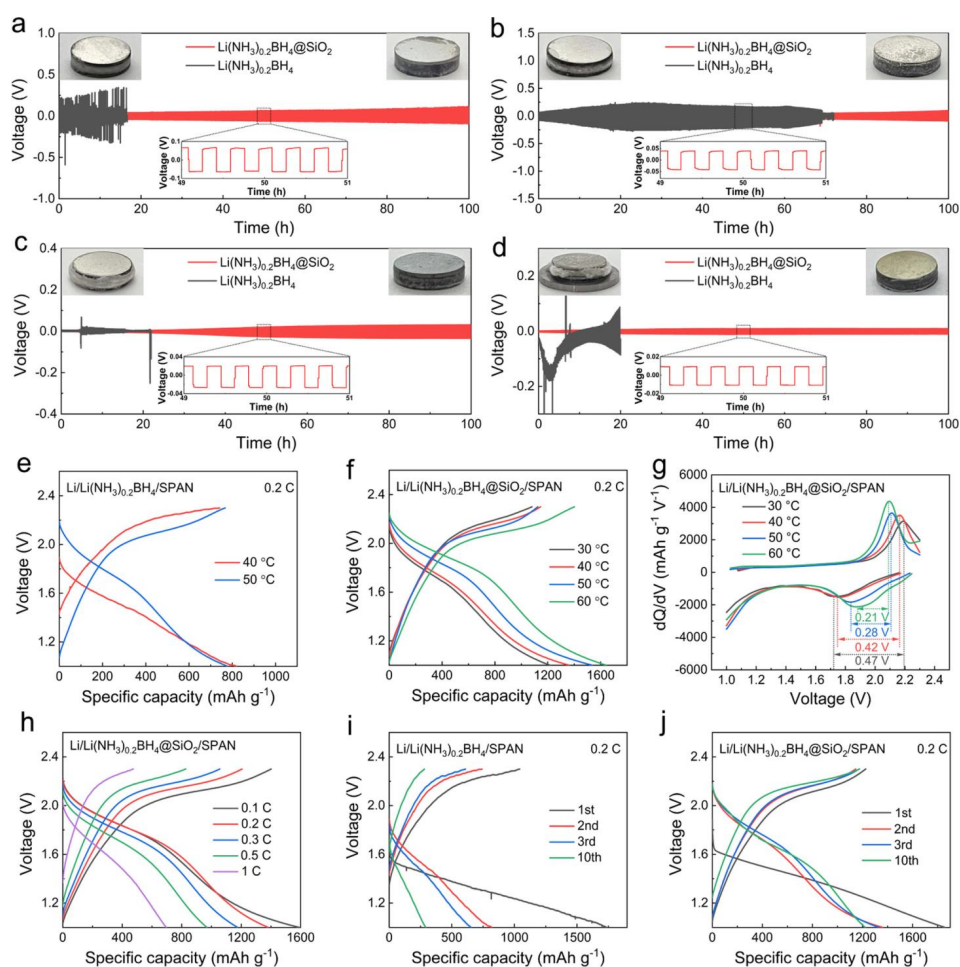


Figure 13. Voltage profiles during galvanostatic Li plating/stripping for the symmetrical Li/Li(NH₃)_{0.2}BH₄/Li and Li/Li(NH₃)_{0.5}BH₄@SiO₂/Li cells at 0.1 mA cm⁻² at 30 °C (a), 40 °C (b), 50 °C (c), and 60 °C (d). Insets: digital images of Li/Li(NH₃)_{0.2}BH₄/Li (left) and Li/Li(NH₃)_{0.5}BH₄@SiO₂/Li (right) after galvanostatic cycling (bottom). (e,f) Voltage profiles during galvanostatic cycles (second cycle) of the Li/Li(NH₃)_{0.2}BH₄/S and Li/Li(NH₃)_{0.5}BH₄@SiO₂/S cells at various temperatures at 0.2C. (g) Differential capacitance curves of curve f. (h) Rate capability of the Li/Li(NH₃)_{0.5}BH₄@SiO₂/S cell at 40 °C at various rates. (i,j) Voltage profiles of Li/Li(NH₃)_{0.2}BH₄/S and Li/Li(NH₃)_{0.5}BH₄@SiO₂/S cells at 40 °C and 0.2C. Reproduced with permission from ref. [54]. Copyright © 2022 American Chemical Society.

Lithium iron phosphate (LiFePO_4) was employed as the cathode active material of a solid-state lithium metal battery with a SSE obtained by adding fullerene to LiBH_4 [42]. The SSE was partially dehydrogenated by heating. The first cycle capacity was very low (20 mAh g^{-1}). An increase in capacity, which reached a value of 73 mAh g^{-1} , was observed as cycling progressed. The solid electrolyte obtained by mixing lithium thiophosphate with LiBH_4 was evaluated in a lithium cell containing $\text{LiNi}_{0.7}\text{Mn}_{0.15}\text{Co}_{0.15}\text{O}_2$ as the cathode [62] (Figure 14). The cycling was initially conducted at 0.05C. At this rate, the measured capacity was 212.3 mAh g^{-1} in charge and 177.5 mAh g^{-1} in discharge with an initial Coulombic efficiency of 83, 6%. When the cell was cycled at higher rates, a good capacity retention was observed; at a discharge rate of 2C, the cell was able to deliver 132.3 mAh g^{-1} (Figure 14b). To evaluate the capacity retention as a function of the cycle number, the cell was cycled at 0.5C. Under these conditions, the cell was capable of cycling for 100 cycles with a low fade rate (Figure 14d).

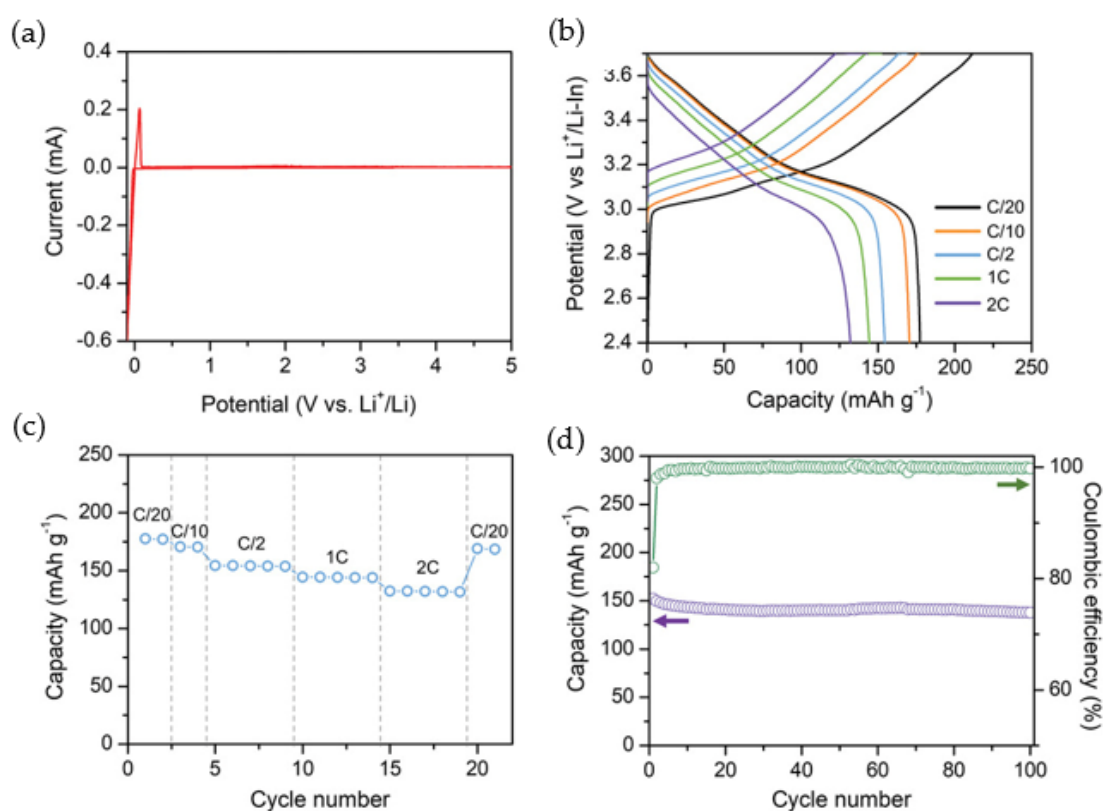


Figure 14. (a) Cyclic voltammogram curves of the Li/thiophosphate- LiBH_4 /SS cell, (b) voltage profiles, (c) rate capability, and (d) capacity as a function of the number of cycles at 0.5C. Reproduced under Creative Commons Attribution License from ref. [62]. Copyright 2023 Wiley.

4. Lithium-Ion Batteries

Studies on anodes, alternative to lithium metal, for the construction of solid-state Li-ion batteries have been focused on metal and metal hydrides which act through the alloy formation or conversion mechanism. Among them, titanium hydride [68], mixture of titanium and magnesium [69,70], vanadium [71], antimony [72], bismuth [73], bismuth telluride [73], bismuth selenide [74], aluminum [75], and titanium/iron [76] have been investigated.

To build a solid-state Li-ion battery with LiBH_4 SSE, the use of titanium hydride (TiH_2) as a negative electrode was tested [68]. The $\text{TiH}_2/\text{LiBH}_4/\text{Li}$ cell was cycled at 120°C with a specific current of 400 mA g^{-1} . The cell showed a first cycle specific capacity of 1094 mAh g^{-1} , which decreased to 878 mAh g^{-1} after 50 cycles. The rate capacity of the TiH_2 composite electrode decreased by about 18% when increasing the specific current

from 400 mA g^{-1} to 1600 mA g^{-1} . $\text{MgH}_2/\text{TiH}_2$ blends have also been proposed as anodes for solid-state Li-ion batteries [69]. When cycled very slowly (0.02C), these blends exhibited specific capacities up to 1700 mAh g^{-1} . A complete sulfur Li-ion cell was constructed by using a mixture of MH_2 and TiH_2 as the negative electrode [70]. To prepare the cathode of the cell, the Li_2S resulting from the electrochemical reduction of the sulfur cathode was employed as the cathode active material. After the first discharge cycle of a Li-S half-cell conducted at 0.02C , the cathode was recuperated and used to assemble the Li-ion cell. The cathode contained approximately 30% molar excess of Li_2S over the amount of metal hydride to compensate for the irreversible capacity lost during the first cycle. The cell was assembled in its discharged state (the starting materials was Li_2S in the cathode and $\text{MgH}_2/\text{TiH}_2$ in the anode). The sulfur/ $\text{MgH}_2\text{-TiH}_2$ cell showed a reversible capacity of 910 mAh g^{-1} (the specific capacity of the cell was referred to the weight of the active material in the negative electrode). Furthermore, the capacity kept at 85% of the initial value in the first 25 charge/discharge cycles (Figure 15).

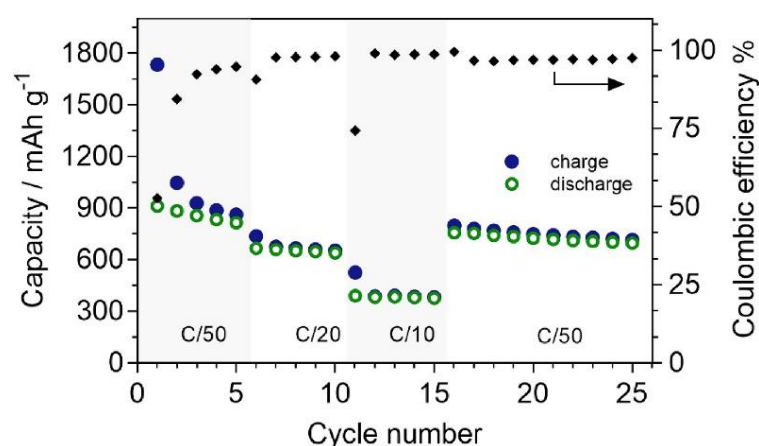


Figure 15. Specific capacity as a function of cycle number of the complete $\text{MgH}_2\text{-TiH}_2/\text{LiBH}_4/\text{S}$ cell cycled at 120°C and various C rates. Reproduced with permission from ref. [70]. Copyright 2017 Elsevier.

Bi and Sb were used as negative electrode materials in solid-state Li-ion batteries with LiBH_4 as SSE. These metals have shown extremely high stability towards the electrolyte, with a high Coulombic efficiency of 90–99% [72]. The specific capacity recorded at the first cycle was 480 and 650 mAh g^{-1} for Bi and Sb, respectively. A capacity fade of about 18% (Bi) and 5% (Sb) affected the electrodes upon cycling. In addition, a 55 nm size Bi_2Te_3 nanosheet was used as the anode active material for solid-state lithium-ion batteries with LiBH_4 as the SSE at 125°C [73]. When cycled at a rate of 0.1C , the anode showed an initial capacity of 555 mAh g^{-1} and 1290 mAh g^{-1} in discharge and charge, respectively. During the electrochemical charge–discharge experiment, the cell was found opened after 11 cycles due to gas evolution. The gas evolution was related to the thermal decomposition of LiBH_4 catalyzed by Bi_2Te_3 . It was suggested that the destabilization of LiBH_4 with Bi_2Te_3 nanosheets is a two-step process with the formation of Li_2Te and Li_3Bi .

Commercial and nanostructured Bi_2Se_3 has been tested as an anode in solid-state lithium-ion batteries [74]. Electrochemical measurements indicated an initial capacity of 621 mAh g^{-1} (in discharge) and 499 mAh g^{-1} (in charge) for the commercial material, which was slightly higher than the nanostructured Bi_2Se_3 (discharge and charge capacity: 594 mAh g^{-1} and 468 mAh g^{-1} , Figure 16a). However, the nanostructured material showed a better cycling stability (Figure 16b).

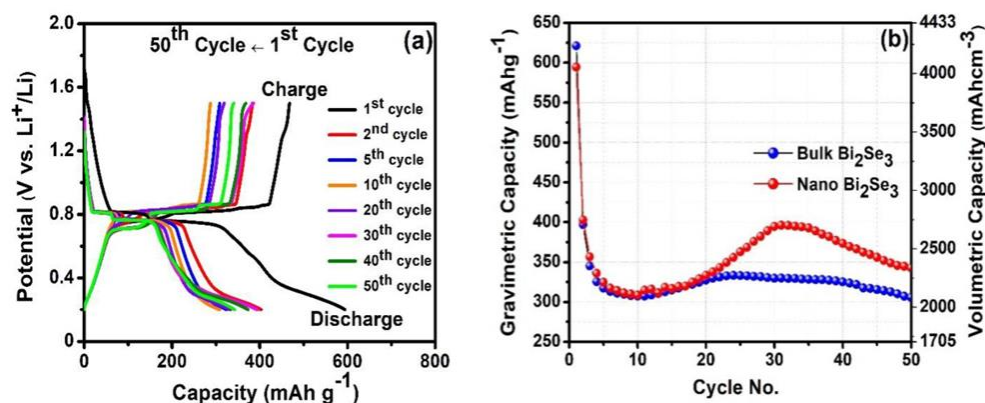


Figure 16. (a) Voltage profile of the Bi₂Se₃-LiBH₄ nanocomposite electrode in the voltage range of 0.2–1.5 V at a rate of 0.1C. (b) Specific capacity as a function of the number of cycles of bulk Bi₂Se₃ and nano Bi₂Se₃. Reproduced with permission from ref. [74]. Copyright 2020 Elsevier.

A simple solid-state pre-lithiation approach has been used to prepare in situ a Li₃AlH₆-Al nanocomposite via a short-circuit electrochemical reduction between LiAlH₄ and Li [75]. This nanocomposite is formed of Al nanograins dispersed in an amorphous Li₃AlH₆ matrix. When tested as an anode in a battery with LiAlH₄ as the SSE, it exhibited a first cycle specific capacity of 2266 mAh g⁻¹, a Coulomb efficiency of 88%, and a capacity retention of 71% in the 100th cycle. With this nanocomposite, a full solid-state cell was made using a LiCoO₂-based cathode which was cycled at 120 °C. The reversible specific capacity of the first cycle was 102 and 1631 mAh g⁻¹, when referring to the weight of the cathode and anode, respectively (Figure 17). The first cycle Coulombic efficiency was 69%. In the following cycles, the cell showed a small capacity decay and a slight increase in the Coulombic efficiencies.

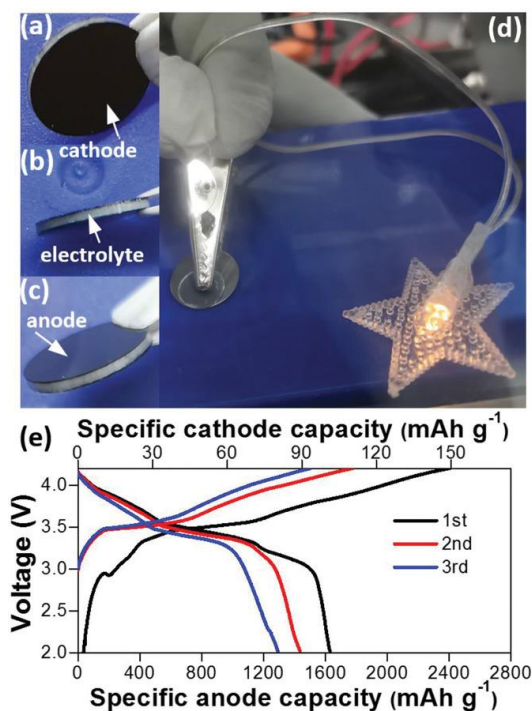


Figure 17. Photographs of the solid-state cell (a) cathode, (b) electrolyte, (c) anode, (d) the entire solid-state cell lighting a LED, and (e) the voltage profiles of the solid-state cell. Reproduced with permission from ref. [75]. Copyright 2020 Wiley.

To evaluate the anode activity of TiFe alloys in the presence of LiH, four different TiFe/LiH ratios were tested by increasing the amount of LiH from 1 to 4 times that of TiFe [76]. The first cycle capacity for the four samples increased by increasing the amount of LiH from 149 to 300 to 441 and finally to 633 mAh g⁻¹. This result confirms that part of the capacity is due to the decomposition of LiH.

5. Discussion

Regardless of the type of electrolyte used, solid-state batteries present a series of problems that must be resolved before placing them on the market. First, the low conductivity of the electrolyte forces to use very thin cathodes containing a high quantity of solid electrolyte. This decreases the energy density of the batteries. The increase in conductivity, consequent to the increase in the operating temperature of the batteries, could increase the thickness of the cathode and decrease the percentage of the electrolyte inside it [77]. Another aspect concerns the effective long-term stability of the electrolyte/lithium interface. Metallic lithium is a strong reductant and parasitic reactions can occur at the interface with the SSE. These reactions primarily affect sulfide-, NASICON-, and garnet-type SSEs, and require engineering strategies to improve interface stability [78]. On the contrary, LiBH₄ proved to be very stable when in contact with Li. For instance, by using a symmetrical Li electrode cell and applying a constant current density of 300 μA cm⁻², a voltage of about 0.2 V was obtained. Only after several cycles a small voltage increase (10 mV), corresponding to a 4.5% increase in cell resistivity, was observed. This increase was attributed to a partial loss of electrical contact at the electrode/electrolyte interface rather than the formation of degradation products [79]. Even the technological aspect concerning the preparation of solid-state batteries still needs to be carefully evaluated. In fact, the difficulties in processing ceramic materials (and among these, also LiBH₄) must be taken into careful consideration. For example, the construction of a 1 kWh battery requires several square meters of surface area, whatever the electrolyte [80]. Sintering processes, used to prepare the SSE, do not produce thicknesses below 30 μm, and high temperatures are required for ceramic electrolytes. Although it was possible to deposit thin films by the vacuum deposition of LiBH₄ [81], this deposition technique is generally of low productivity and therefore expensive. Unlike conventional battery systems, solid-state batteries need at least 10 MPa (or greater) of pressure to allow for stable cycling and avoid contact loss or dendrite formation [82]. This requires extensive product design and manufacturing line changes for solid-state batteries, which could potentially increase overall costs. Current LIBs have safety issues due to the fire hazards related to the organic solvents they contain. Although solid-state batteries are theoretically safer than LIBs, this greater safety has yet to be demonstrated, especially for batteries operating above 150 °C [83]. Compared to other SSEs, LiBH₄ is thermally more stable. The thermal analysis conducted on LiBH₄ was studied by Fedeneva et al. [84]. Three endothermic effects were observed during heating: at 108–112, 268–286 and 483–492 °C. The first effect is reversible since it is related to the polymorphic transformation of LiBH₄. The second peak at 268–286 °C coincides to the melting of LiBH₄ that is accompanied by a slight decomposition, liberating about 2 wt.% of the hydrogen contained in the borohydride. At higher temperatures, the main evolution of hydrogen is witnessed with the release of about 80% of the hydrogen contained in the compound. However, substances mixed with LiBH₄ to increase the ionic conductivity can modify this behavior. For example, the addition of 25 wt.% SiO₂ has been observed to catalyze the decomposition reaction of LiBH₄ and lower the temperature for all three hydrogen desorption characteristics [85]. LiBH₄ has a very low specific gravity (0.667 g cm⁻³) compared to other solid electrolytes, and this represents an advantage since it is reflected in a higher energy density of the cell. Finally, to evaluate the possibility of using the LiBH₄ as the SSE, it is necessary to consider its cost as well as the possible large-scale production. LiBH₄ is made up of lithium and boron, both of which are not very common on the earth's crust but easily available since they are concentrated in surface deposits. The synthesis of the material is not complicated, but involves the electrochemical reduction of lithium,

which is energetically expensive. The market cost of LiBH_4 is around $\$0.60\text{--}0.75\text{ g}^{-1}$ [86]. Considering the density of the material, we have a cost of $\$0.4\text{--}0.5\text{ cm}^{-3}$. To cover an area of 1 m^2 with an electrolyte thickness of $10\text{ }\mu\text{m}$, 10 cm^3 of LiBH_4 is required for a cost of $\$4\text{--}5$. This cost is lower than the one originally proposed by McCloskey [87] and later indicated by the US Department of Energy's Agency for Energy (ARPA-E), which is set at a maximum of $\$10\text{ m}^{-2}$ [88].

6. Conclusions

The studies conducted in the last 10 years have aimed to increase the ionic conductivity of LiBH_4 to use it as an SSE in solid-state batteries operating at room temperature. The effort was productive as it demonstrated that LiBH_4 doping can lead to the realization of SSEs with room temperature conductivity comparable to that of the alkyl carbonates used in liquid-electrolyte lithium-ion batteries. Furthermore, the performance of solid-state batteries made using LiBH_4 -based SSE has also led to satisfactory results. Although further experiments are needed to evaluate long-term stability, the results obtained seem promising and suggest that LiBH_4 -based solid-state batteries could be susceptible to future industrial development.

Funding: Part of this research was funded by the Ministry of Enterprise and Made in Italy within the second important project of common European interest in the battery sector (IPCEI Batterie 2) and by the Ministry of the Environment within the PTR 2022–2024.

Data Availability Statement: Not applicable.

Conflicts of Interest: The author declares no conflict of interest.

References

1. Scrosati, B. History of lithium batteries. *J. Solid State Electrochem.* **2011**, *15*, 1623–1630. [CrossRef]
2. Reddy, M.V.; Mauger, A.; Julien, C.M.; Paoletta, A.; Zaghib, K. Brief History of Early Lithium-Battery Development. *Materials* **2020**, *13*, 1884. [CrossRef] [PubMed]
3. Scrosati, B.; Garche, J. Lithium batteries: Status, prospects and future. *J. Power Sources* **2010**, *195*, 2419–2430. [CrossRef]
4. La Monaca, A.; De Giorgio, F.; Soavi, F.; Tarquini, G.; Di Carli, M.; Prosini, P.P.; Arbizzani, C. 1,3-Dioxolane: A strategy to improve electrode interfaces in Lithium ion and lithium-sulfur batteries. *ChemElectroChem* **2018**, *5*, 1272–1278. [CrossRef]
5. Janek, J.; Zeier, W.G. A solid future for battery development. *Nat. Energy* **2016**, *1*, 16141. [CrossRef]
6. Kato, Y.; Hori, S.; Saito, T.; Suzuki, K.; Hirayama, M.; Mitsui, A.; Yonemura, M.; Iba, H.; Kanno, R. High-power all-solid-state batteries using sulfide superionic conductors. *Nat. Energy* **2016**, *1*, 16030. [CrossRef]
7. Han, X.; Gong, Y.; Fu, K.; He, X.; Hitz, G.T.; Dai, J.; Pearse, A.; Liu, B.; Wang, H.; Rublo, G.; et al. Negating interfacial impedance in garnet-based solid-state Li metal batteries. *Nat. Mater.* **2017**, *16*, 572–579. [CrossRef]
8. Han, F.; Gao, T.; Zhu, Y.; Gaskell, K.J.; Wang, C. A battery made from a single material. *Adv. Mater.* **2015**, *27*, 3473–3483. [CrossRef]
9. Zhang, J.; Zhao, J.; Yue, L.; Wang, Q.; Chai, J.; Liu, Z.; Zhou, X.; Li, H.; Guo, Y.; Cui, G.; et al. Safety-reinforced poly(propylene carbonate)-based all-solid-state polymer electrolyte for ambient-temperature solid polymer lithium batteries. *Adv. Energy Mater.* **2015**, *5*, 1501082. [CrossRef]
10. Christie, A.M.; Lilley, S.J.; Staunton, E.; Andreev, Y.G.; Bruce, P.G. Increasing the conductivity of crystalline polymer electrolytes. *Nature* **2005**, *433*, 50–53. [CrossRef]
11. Lin, D.; Liu, W.; Liu, Y.; Lee, H.R.; Hsu, P.-C.; Liu, K.; Cui, Y. High ionic conductivity of composite solid polymer electrolyte via in situ synthesis of monodispersed SiO_2 nanospheres in poly(ethylene oxide). *Nano Lett.* **2016**, *16*, 459–465. [CrossRef] [PubMed]
12. Appetecchi, G.B.; Croce, F.; Dautzenberg, G.; Mastragostino, M.; Ronci, F.; Scrosati, B.; Soavi, F.; Zanelli, A.; Alessandrini, F.; Prosini, P.P. Composite polymer electrolytes with improved lithium metal electrode interfacial properties: I. Electrochemical properties of dry PEO-LiX systems. *J. Electrochem. Soc.* **1998**, *145*, 4126–4132. [CrossRef]
13. Tachez, M.; Malugani, J.-P.; Mercier, R.; Robert, G. Ionic conductivity of and phase transition in lithium thiophosphate Li_3PS_4 . *Solid State Ion.* **1984**, *14*, 181–185. [CrossRef]
14. Campanella, D.; Daniel Belanger, D.; Paoletta, A. Beyond garnets, phosphates and phosphosulfides solid electrolytes: New ceramic perspectives for all solid lithium metal batteries. *J. Power Sources* **2021**, *482*, 228949. [CrossRef]
15. Tatsumisago, M.; Yamashita, H.; Hayashi, A.; Morimoto, H.; Minami, T.J. Preparation and structure of amorphous solid electrolytes based on lithium sulfide. *Non-Cryst. Solids* **2000**, *274*, 30–38. [CrossRef]
16. Aono, H.; Sugimoto, E.; Sadaoka, Y.; Imanaka, N.; Adachi, G. High Li^+ conducting ceramics. *Acc. Chem. Res.* **1994**, *27*, 265–270. [CrossRef]

17. Tomita, Y.; Matsushita, H.; Kobayashi, K.; Maeda, Y.; Yamada, K. Substitution effect of ionic conductivity in lithium ion conductor, $\text{Li}_3\text{InBr}_{6-x}\text{Cl}_x$. *Solid State Ion.* **2008**, *179*, 867–870. [CrossRef]
18. Liang, C.C. Conduction Characteristics of the Lithium Iodide-Aluminum Oxide Solid Electrolytes. *J. Electrochem. Soc.* **1973**, *120*, 1289–1292. [CrossRef]
19. Maekawa, H.; Tanaka, R.; Sato, T.; Fujimaki, Y.; Yamamura, T. Size-dependent ionic conductivity observed for ordered mesoporous alumina-LiI composite. *Solid State Ion.* **2004**, *175*, 281–285. [CrossRef]
20. Guo, Z.; Ye, C.; Zhao, T.; Wu, W.; Kou, W.; Zhang, Y.; Dong, W.; Li, W.; Wang, J. Thin lamellar $\text{Li}_7\text{La}_3\text{Zr}_2\text{O}_{12}$ solid electrolyte with $\text{g-C}_3\text{N}_4$ as grain boundary modifier for high-performance all-solid-state lithium battery. *J. Power Sources* **2023**, *562*, 232784. [CrossRef]
21. Kawahara, K.; Ishikawa, R.; Nakayama, K.; Higashi, T.; Kimura, T.; Ikuhara, Y.H.; Shibata, N.; Ikuhara, Y. Fast Li-ion conduction at grain boundaries in (La, Li)NbO₃ polycrystals. *J. Power Sources* **2019**, *441*, 227187. [CrossRef]
22. Shiiba, H.; Zettsu, N.; Yamashita, M.; Onodera, H.; Jalem, R.; Nakayama, M.; Teshima, K. Molecular dynamics studies on the lithium ion conduction behaviors depending on tilted grain boundaries with various symmetries in garnet-type $\text{Li}_7\text{La}_3\text{Zr}_2\text{O}_{12}$. *J. Phys. Chem. C* **2018**, *122*, 21755–21762. [CrossRef]
23. He, X.; Zhu, Y.; Mo, Y. Origin of fast ion diffusion in super-ionic conductors. *Nat. Commun.* **2017**, *8*, 15893. [CrossRef]
24. Peng, L.; Yu, C.; Wei, C.; Liao, C.; Chen, S.; Zhang, L.; Cheng, S.; Xie, J. Recent Progress on Lithium Argyrodite Solid-State Electrolytes. *Wuli Huaxue Xuebao/Acta Phys.-Chim. Sin.* **2023**, *39*, 2211034. [CrossRef]
25. Hori, S.; Kanno, R.; Sun, X.; Song, S.; Hirayama, M.; Hauck, B.; Dippon, M.; Dierickx, S.; Ivers-Tiffée, E. Understanding the impedance spectra of all-solid-state lithium battery cells with sulfide superionic conductors. *J. Power Sources* **2023**, *556*, 232450. [CrossRef]
26. Nakamori, Y.; Orimo, S.-I.; Tsutaoka, T. Dehydrogenation reaction of metal hydrides and alkali borohydrides enhanced by microwave irradiation. *Appl. Phys. Lett.* **2006**, *88*, 112104. [CrossRef]
27. Brown, H.C. From Little Acorns to Tall Oaks from Boranes through Organoboranes. Nobel Lecture. 8 December 1979. Available online: <https://www.nobelprize.org/uploads/2018/06/brown-lecture.pdf> (accessed on 27 April 2023).
28. Schlesinger, H.C.; Brown, H.R. Metallo Borohydrides. III. Lithium Borohydride. *J. Am. Chem. Soc.* **1940**, *62*, 3429–3435. [CrossRef]
29. Schlesinger, H.C.; Brown, H.R.; Hoekstra, L.R. Reactions of Diborane with Alkali Metal Hydrides and Their Addition Compounds. New Syntheses of Borohydrides. Sodium and Potassium Borohydrides. *J. Am. Chem. Soc.* **1953**, *75*, 199–204. [CrossRef]
30. Kollonitsch, J.; Fuchs, O.; Gábor, V. Alkaline-earth borohydrides and their applications in organic syntheses. *Nature* **1955**, *175*, 346. [CrossRef]
31. Picasso, C.V.; Safin, D.A.; Dovgaliuk, I.; Devred, F.; Debecker, D.; Li, H.W.; Proost, J.; Filinchuk, Y. Reduction of CO₂ with KBH₄ in solvent-free conditions. *Int. J. Hydrogen Energy* **2016**, *41*, 14377–14386. [CrossRef]
32. Orimo, S.; Nakamori, Y.; Eliseo, J.R.; Züttel, A.; Jensen, C.M. Complex hydrides for hydrogen storage. *Chem. Rev.* **2007**, *107*, 4111–4132.
33. Züttel, A.; Wenger, P.; Rentsch, S.; Sudan, P.; Mauron, P.; Emmenegger, C. LiBH₄ a new hydrogen storage material. *J. Power Sources* **2003**, *118*, 1–7. [CrossRef]
34. Prosini, P.P.; Gislou, P. Water consumption during solid state sodium borohydride hydrolysis, International. *Int. J. Hydrogen Energy* **2010**, *35*, 12234–12238. [CrossRef]
35. Matsuo, M.; Nakamori, Y.; Orimo, S.; Maekawa, H.; Takamura, H. Lithium superionic conduction in lithium borohydride accompanied by structural transition. *Appl. Phys. Lett.* **2007**, *91*, 224103. [CrossRef]
36. Pang, Y.; Liu, Y.; Yang, J.; Zheng, S.; Wang, C. Hydrides for solid-state batteries: A review. *Mater. Today Nano* **2022**, *18*, 100194. [CrossRef]
37. Skripov, A.V.; Soloninin, A.V.; Filinchuk, Y.; Chernyshov, D. Nuclear Magnetic Resonance Study of the Rotational Motion and the Phase Transition in LiBH₄. *J. Phys. Chem. C* **2008**, *112*, 18701–18705. [CrossRef]
38. Maekawa, H.; Matsuo, M.; Takamura, H.; Ando, M.; Noda, Y.; Karahashi, T.; Orimo, S. Halide-Stabilized LiBH₄, a Room-Temperature Lithium Fast-Ion Conductor. *J. Am. Chem. Soc.* **2009**, *131*, 894–895. [CrossRef]
39. Yamauchi, A.; Sakuda, A.; Hayashi, A.; Tatsumisago, M. Preparation and ionic conductivities of (100 - x)(0.75Li₂S-0.25P₂S₅)·xLiBH₄ glass electrolytes. *J. Power Sources* **2013**, *244*, 707–710. [CrossRef]
40. El Kharbachi, A.; Sorby, M.H.; Nygard, M.M.; Hauback, B.C. Borohydride-based Solid-state Electrolytes for Lithium Batteries. In Proceedings of the 2019 7th International Renewable and Sustainable Energy Conference, IRSEC 2019, Agadir, Morocco, 27–30 November 2019; p. 750.
41. Teprovich, J.A., Jr.; Colón-Mercado, H.R.; Ward, P.A.; Peters, B.; Giri, S.; Zhou, J.; Greenway, S.; Compton, R.N.; Jena, P.; Zidan, R. Experimental and Theoretical Analysis of Fast Lithium Ionic Conduction in a LiBH₄-C₆₀ Nanocomposite. *J. Phys. Chem. C* **2014**, *118*, 21755–21761. [CrossRef]
42. Santos, J.A.; Simon, P.; Bernot, A.R.; Babasi, C.; Ward, P.A.; Hwang, S.-J.; Zidan, R.; Teprovich, J.A. Synergistic effect of nanoionic destabilization and partial dehydrogenation for enhanced ionic conductivity in MBH₄-C₆₀ (M = Li⁺, Na⁺) nanocomposites. *J. Solid State Electrochem.* **2021**, *25*, 1441–1452. [CrossRef]
43. Blanchard, D.; Nale, A.; Sveinbjörnsson, D.; Eggenhuisen, T.M.; Verkuijlen, M.H.W.; Suwarno; Vegge, T.; Kentgens, A.P.M.; de Jongh, P.E. Nanoconfined LiBH₄ as a Fast Lithium Ion Conductor. *Adv. Funct. Mater.* **2015**, *25*, 184–192. [CrossRef]

44. Verkuijlen, M.H.W.; Ngene, P.; de Kort, D.W.; Barré, C.; Nale, A.; van Eck, E.R.H.; van Bentum, P.J.M.; de Jongh, P.E.; Kentgens, A.P.M. Nanoconfined LiBH_4 and Enhanced Mobility of Li^+ and BH_4^- Studied by Solid-State NMR. *J. Phys. Chem. C* **2012**, *116*, 22169–22178. [[CrossRef](#)]
45. Yang, G.; Xie, C.; Li, Y.; Li, H.-W.; Liu, D.; Chen, J.; Zhang, Q. Enhancement of the ionic conductivity of lithium borohydride by silica supports. *Dalton Trans.* **2021**, *50*, 15352–15358. [[CrossRef](#)] [[PubMed](#)]
46. Ngene, P.; Lambregts, S.F.H.; Blanchard, D.; Vegge, T.; Sharma, M.; Hagemann, H.; De Jongh, P.E. The influence of silica surface groups on the Li-ion conductivity of $\text{LiBH}_4/\text{SiO}_2$ nanocomposites. *Phys. Chem. Chem. Phys.* **2019**, *21*, 22456–22466. [[CrossRef](#)]
47. Lambregts, S.F.H.; Van Eck, E.R.H.; Suwarno; Ngene, P.; De Jongh, P.E.; Kentgens, A.P.M. Phase Behavior and Ion Dynamics of Nanoconfined LiBH_4 in Silica (2019). *J. Phys. Chem. C* **2019**, *123*, 25559–25569. [[CrossRef](#)]
48. Lu, F.; Pang, Y.; Zhu, M.; Han, F.; Yang, J.; Fang, F.; Sun, D.; Zheng, S.; Wang, C. A High-Performance Li–B–H Electrolyte for All-Solid-State Li Batteries. *Adv. Funct. Mater.* **2019**, *29*, 1809219. [[CrossRef](#)]
49. Zhang, X.; Zhang, T.; Shao, Y.; Cao, H.; Liu, Z.; Wang, S.; Zhang, X. Composite Electrolytes Based on Poly(Ethylene Oxide) and Lithium Borohydrides for All-Solid-State Lithium–Sulfur Batteries. *ACS Sustain. Chem. Eng.* **2021**, *9*, 5396–5404. [[CrossRef](#)]
50. Takano, A.; Oikawa, I.; Kamegawa, A.; Takamura, H. Enhancement of the lithium-ion conductivity of LiBH_4 by hydration. *Solid State Ion.* **2016**, *285*, 47–50. [[CrossRef](#)]
51. Zhang, T.; Wang, Y.; Song, T.; Miyaoka, H.; Shinzato, K.; Miyaoka, H.; Ichikawa, T.; Shi, S.; Zhang, X.; Isobe, S.; et al. Ammonia, a Switch for Controlling High Ionic Conductivity in Lithium Borohydride Ammoniates. *Joule* **2018**, *2*, 1522–1533. [[CrossRef](#)]
52. Yan, Y.; Grinderslev, J.B.; Lee, Y.-S.; Jørgensen, M.; Cho, Y.W.; Černý, R.; Jensen, T.R. Ammonia-assisted fast Li-ion conductivity in a new hemiammine lithium borohydride, $\text{LiBH}_4 \cdot 1/2\text{NH}_3$. *Chem. Comm.* **2020**, *56*, 3971–3974. [[CrossRef](#)]
53. Mohtadi, R. High Li-Ion Conductivity in a Hydride-type Solid-State Electrolyte: The Ammonia Effect. *Chem* **2018**, *4*, 1770–1772. [[CrossRef](#)]
54. Liu, Z.; Zhang, T.; Ju, S.; Ji, Y.; Hu, Z.; Lv, Y.; Xia, G.; Yu, X. Fast Ionic Migration from Bulk to Interface in the $\text{Li}(\text{NH}_3)_x\text{BH}_4@ \text{SiO}_2$ Composite. *ACS Appl. Energy Mater.* **2022**, *5*, 14301–14310. [[CrossRef](#)]
55. Yan, Y.; Kühnel, R.-S.; Remhof, A.; Duchêne, L.; Reyes, E.C.; Rentsch, D.; Łodziana, Z.; Battaglia, C. A Lithium Amide-Borohydride Solid-State Electrolyte with Lithium-Ion Conductivities Comparable to Liquid Electrolytes. *Adv. Energy Mater.* **2017**, *7*, 1700294. [[CrossRef](#)]
56. Zhao, W.; Zhang, R.; Li, H.; Zhang, Y.; Wang, Y.; Wu, C.; Yan, Y.; Chen, Y. Li-Ion Conductivity Enhancement of $\text{LiBH}_4 \cdot x\text{NH}_3$ with In Situ Formed Li_2O Nanoparticles. *ACS Appl. Mater. Interfaces* **2021**, *13*, 31635–31641. [[CrossRef](#)] [[PubMed](#)]
57. Liu, H.; Ren, Z.; Zhang, X.; Hu, J.; Gao, M.; Pan, H.; Liu, Y. Incorporation of Ammonia Borane Groups in the Lithium Borohydride Structure Enables Ultrafast Lithium Ion Conductivity at Room Temperature for Solid-State Batteries. *Chem. Mater.* **2020**, *32*, 32671–32678. [[CrossRef](#)]
58. Grinderslev, J.B.; Skov, L.N.; Andreasen, J.G.; Ghorwal, S.; Skibsted, J.; Jensen, T.R. Methylamine Lithium Borohydride as Electrolyte for All-Solid-State Batteries. *Angew. Chem. Int. Ed. Engl.* **2022**, *61*, e202203484. [[CrossRef](#)] [[PubMed](#)]
59. Luo, X.; Rawal, A.; Cazorla, C.; Aguey-Zinsou, K.-F. Facile Self-Forming Superionic Conductors Based on Complex Borohydride Surface Oxidation. *Adv. Sustain. Syst.* **2020**, *4*, 1900113. [[CrossRef](#)]
60. Gulino, V.; Brighi, M.; Murgia, F.; Ngene, P.; de Jongh, P.; Černý, R.; Baricco, M. Room-Temperature Solid-State Lithium-Ion Battery Using a LiBH_4 – MgO Composite Electrolyte. *ACS Appl. Energy Mater.* **2021**, *4*, 1228–1236. [[CrossRef](#)]
61. de Kort, L.M.; Gulino, V.; Blanchard, D.; Ngene, P. Effects of LiBF_4 Addition on the Lithium-Ion Conductivity of LiBH_4 . *Molecules* **2022**, *27*, 2187. [[CrossRef](#)]
62. Jang, Y.-J.; Seo, H.; Lee, Y.-S.; Kang, S.; Cho, W.; Cho, Y.W.; Kim, J.-H. Lithium Superionic Conduction in BH_4 -Substituted Thiophosphate Solid Electrolytes. *Adv. Sci.* **2023**, *10*, 2204942. [[CrossRef](#)]
63. Takahashi, K.; Hattori, K.; Yamazaki, T.; Takada, K.; Matsuo, M.; Orimo, S.; Maekawa, H.; Takamura, H. All-solid-state lithium battery with LiBH_4 solid electrolyte. *J. Power Sources* **2013**, *226*, 61–64. [[CrossRef](#)]
64. Suzuki, S.; Kawaji, J.; Yoshida, K.; Unemoto, A.; Orimo, S. Development of complex hydride-based all-solid-state lithium ion battery applying low melting point electrolyte. *J. Power Sources* **2017**, *359*, 97–103. [[CrossRef](#)]
65. Tripathi, B.; Patodia, T.; Jain, A.; Ichikawa, T.; Katiyar, R. Optimization of Cycling Performance for CNT Impregnated Sulfur Composite Cathode Using LiBH_4 as Solid Electrolyte for All Solid State Li-S Batteries. *ECS Trans.* **2021**, *104*, 53–60. [[CrossRef](#)]
66. Patodia, T.; Gupta, M.K.; Singh, R.; Ichikawa, T.; Jain, A.; Tripathi, B. Electrochemical Performance of Graphene-Modulated Sulfur Composite Cathodes Using LiBH_4 Electrolyte for All-Solid-State Li-S Battery. *Energies* **2021**, *14*, 7362. [[CrossRef](#)]
67. Takahashi, K.; Maekawa, H.; Takamura, H. Effects of intermediate layer on interfacial resistance for all-solid-state lithium batteries using lithium borohydride. *Solid State Ion.* **2014**, *262*, 179–182. [[CrossRef](#)]
68. Kawahito, K.; Zeng, L.; Ichikawa, T.; Miyaoka, H.; Kojima, Y. Electrochemical Performance of Titanium Hydride for Bulk-Type All-Solid-State Lithium-Ion Batteries. *Mater. Trans.* **2016**, *57*, 755–757. [[CrossRef](#)]
69. Dao, A.H.; Berti, N.; López-Aranguren, P.; Zhang, J.; Cuevas, F.; Jordy, C.; Latroche, M. Electrochemical properties of MgH_2 – TiH_2 nanocomposite as active materials for all-solid-state lithium batteries. *J. Power Sources* **2018**, *397*, 143–149. [[CrossRef](#)]
70. López-Aranguren, P.; Berti, N.; Dao, A.H.; Zhang, J.; Cuevas, F.; Latroche, M.; Jordy, C. An all-solid-state metal hydride–Sulfur lithium-ion battery. *J. Power Sources* **2017**, *357*, 56–60. [[CrossRef](#)]
71. Matsumura, Y.; Takagishi, K.; Miyaoka, H.; Ichikawa, T. Vanadium Hydride as Conversion Type Negative Electrode for All-Solid-State Lithium-Ion-Battery. *Mat. Trans.* **2019**, *60*, 2183–2187. [[CrossRef](#)]

72. Kumari, P.; Sharma, K.; Pal, P.; Kumar, M.; Ichikawa, T.; Jain, A. Highly efficient & stable Bi & Sb anodes using lithium borohydride as solid electrolyte in Li-ion batteries. *RSC Adv.* **2019**, *9*, 13077–13081.
73. Kumari, P.; Pal, P.; Shinzato, K.; Awasthi, K.; Ichikawa, T.; Jain, A.; Kumar, M. Nanostructured Bi₂Te₃ as anode material as well as a destabilizing agent for LiBH₄. *Int. J. Hydrogen Energy* **2020**, *45*, 16992–16999. [[CrossRef](#)]
74. Kumari, P.; Singh, R.; Awasthi, K.; Ichikawa, T.; Kumar, M.; Jain, A. Highly stable nanostructured Bi₂Se₃ anode material for all solid-state lithium-ion batteries. *J. Alloys Compd.* **2020**, *838*, 155403. [[CrossRef](#)]
75. Pang, Y.; Wang, X.; Shi, X.; Xu, F.; Sun, L.; Yang, J.; Zheng, S. Solid-State Preolithiation Enables High-Performance Li-Al-H Anode for Solid-State Batteries. *Adv. Energy Mater.* **2020**, *10*, 1902795. [[CrossRef](#)]
76. Singh, R.; Fernando, C.B.; Ichikawa, T.; Jain, A. Conversion reaction of TiFe hydride as anode material for all-solid-state Lithium-ion batteries. *Mater. Lett. X* **2021**, *10*, 100067.
77. Janek, J.; Zeier, W.G. Challenges in speeding up solid-state battery development. *Nat. Energy* **2023**, *8*, 230–240. [[CrossRef](#)]
78. Paul, P.P.; Chen, B.-R.; Langevin, S.A.; Dufek, E.J.; Nelson Weker, J.; Ko, J.S. Interfaces in all solid state Li-metal batteries: A review on instabilities, stabilization strategies, and scalability. *Energy Storage Mater.* **2022**, *45*, 969–1001. [[CrossRef](#)]
79. Das, S.; Ngene, P.; Norby, P.; Vegge, T.; De Jongh, P.E.; Blanchard, D. All-solid-state lithium-sulfur battery based on a nanoconfined LiBH₄ electrolyte. *J. Electrochem. Soc.* **2016**, *163*, A2029–A2034. [[CrossRef](#)]
80. Mauger, A.; Julien, C.M.; Paolella, A.; Armand, M.; Zaghib, K. Building Better Batteries in the Solid State: A Review. *Materials* **2019**, *12*, 3892. [[CrossRef](#)]
81. Oguchi, H.; Kim, S.; Maruyama, S.; Horisawa, Y.; Takagi, S.; Sato, T.; Shimizu, R.; Matsumoto, Y.; Hitosugi, T.; Orimo, S. Epitaxial Film Growth of LiBH₄ via Molecular Unit Evaporation. *ACS Appl. Electron. Mater.* **2019**, *1*, 1792–1796. [[CrossRef](#)]
82. Zaman, W.; Hatzell, K.B. Processing and manufacturing of next generation lithium-based all solid-state batteries. *Curr. Opin. Solid State Mater. Sci.* **2022**, *26*, 101003. [[CrossRef](#)]
83. Kim, T.; Kim, K.; Lee, S.; Song, G.; Jung, M.S.; Lee, K.T. Thermal runaway behavior of Li₆PS₅Cl solid electrolytes for LiNi_{0.8}Co_{0.1}Mn_{0.1}O₂ and LiFePO₄ in all-solid-state batteries. *Chem. Mater.* **2022**, *34*, 9159–9171. [[CrossRef](#)]
84. Fedneva, E.M.; Alpatova, V.L.; Mikheeva, V.I. Thermal stability of lithium borohydride. *Russ. J. Inorg. Chem.* **1964**, *9*, 826–827.
85. Züttel, A.; Rentsch, S.; Fischer, P.; Wenger, P.; Sudan, P.; Mauron, P.; Emmenegger, C. Hydrogen storage properties of LiBH₄. *J. Alloys Compd.* **2003**, *356–357*, 515–520. [[CrossRef](#)]
86. Selling Price of LiBH₄. Available online: <https://www.alibaba.com/showroom/libh4.html> (accessed on 27 April 2023).
87. McCloskey, B.D. Attainable Gravimetric and Volumetric Energy Density of Li-S and Li Ion Battery Cells with Solid Separator-Protected Li Metal Anodes. *J. Phys. Chem. Lett.* **2015**, *6*, 4581–4588. [[CrossRef](#)]
88. Sendek, A.D.; Cheon, G.; Pasta, M.; Reed, E.J. Quantifying the Search for Solid Li-Ion Electrolyte Materials by Anion: A Data-Driven Perspective. *J. Phys. Chem. C* **2020**, *124*, 8067–8079. [[CrossRef](#)]

Disclaimer/Publisher’s Note: The statements, opinions and data contained in all publications are solely those of the individual author(s) and contributor(s) and not of MDPI and/or the editor(s). MDPI and/or the editor(s) disclaim responsibility for any injury to people or property resulting from any ideas, methods, instructions or products referred to in the content.